Electronic Supplementary Material (ESI) for Sustainable Energy & Fuels.


# Valence state modulation of $Mn/FePO_4$ nanostructures for oxygen reduction reactions

*Zubair Ahmed,*[a] *Krishnakanth,*[a] *Parrydeep K. Sachdeva,*[a] *Rajdeep Kaur,*[a] *Shilpa Kumari,*[a] *Chandan Bera,*[a] *and Vivek Bagchi**[a].

[a]Institute of Nano Science and Technology (INST) Sector-81, Knowledge City, Sahibzada Ajit Singh Nagar, Punjab, Pin - 140306.

* To whom correspondence should be addressed. Email: bagchiv@inst.ac.in Tel: +91-172-2210075 Ext. 311 Fax: +91-172-2211074

# Supporting information

**S1 Theoretical details:**

The convergence threshold for energy is set at $10^{-4}$ eV. Structures are optimized using selective dynamics as performed in VASP. The supercell was constructed with 120 atoms including planar graphene sheet with dimensions a = 17.1 Å; b = 14.8 Å; c = 15 Å for the calculation. In c-crystallographic direction 15 Å vacuum is provided to prevent the interaction of periodic layers of graphene. The supercell was studied for energy convergence and accordingly, the plane wave cut off energy was set to 520 eV with 7x7x1 gamma-centered K-mesh. Table below represents the total energy of all the systems: The supercell was studied for energy convergence and accordingly, the plane wave cut off energy was set to 520 eV with 7x7x1 gamma-centered K-mesh. Table below represents the total energy of all the systems.

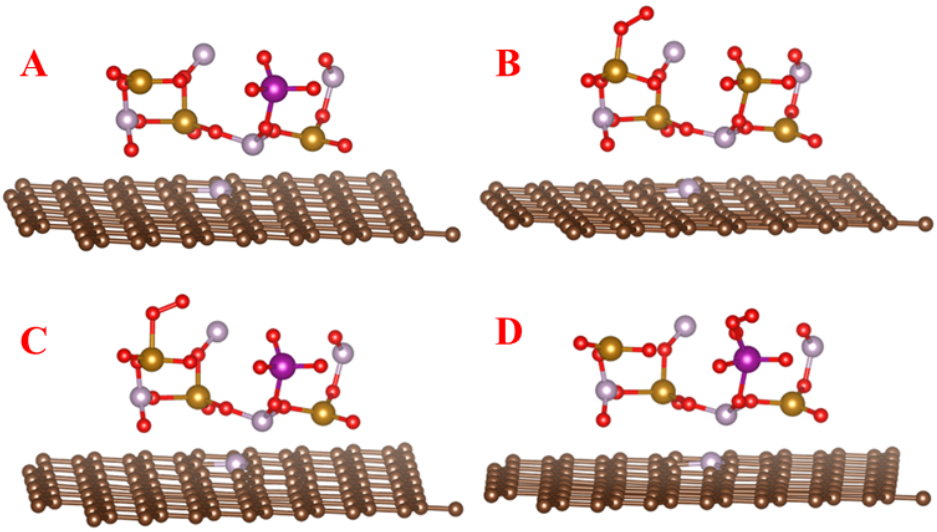


**Figure S1** (A) Relaxed geometries of Mn-doped $FePO_4$ and Oxygen adsorption on Fe-atoms in (B) $FePO_4$ (C) Mn-doped $FePO_4$ and (D) Oxygen adsorption on Mn-atoms in Mn-doped $FePO_4$ all placed on PRGO surface

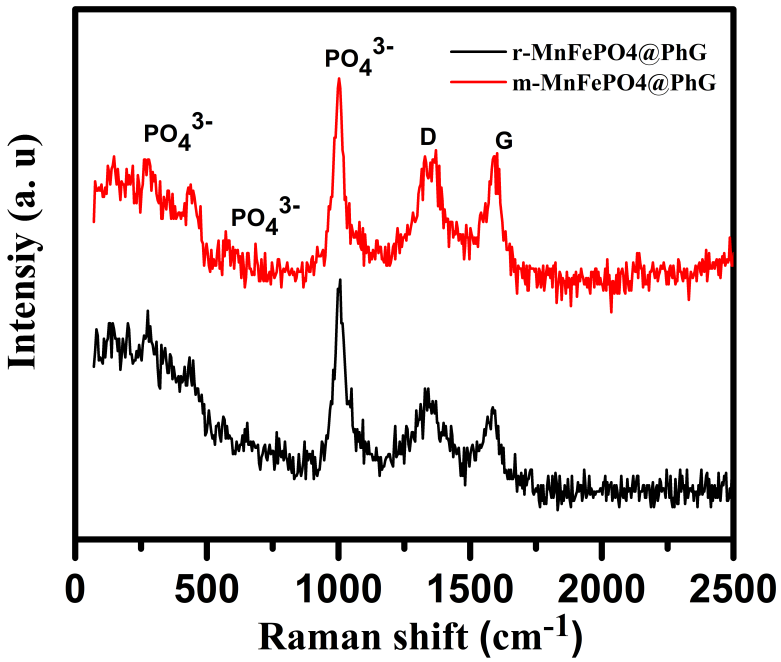


**Figure S2:** Raman spectra of r-MnFePO$_4$@PhG and m-MnFePO$_4$@PhG composites

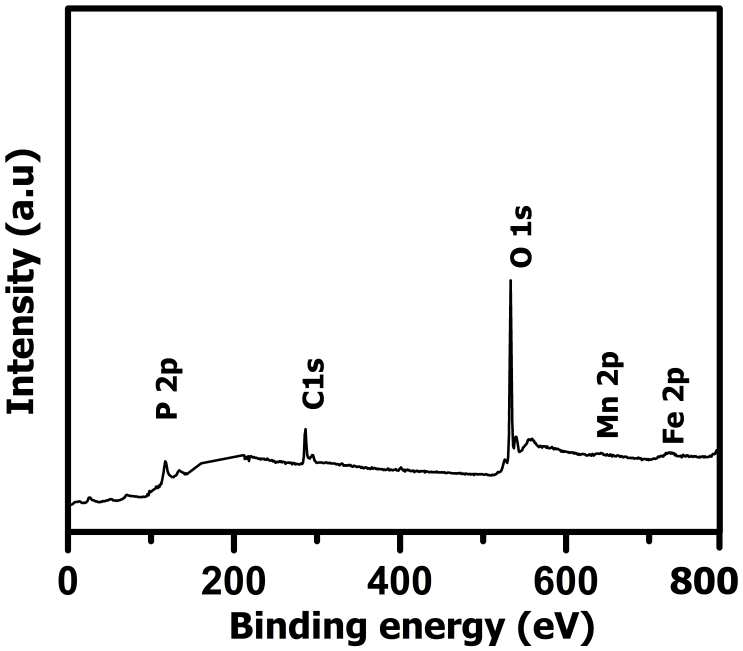


**Figure S3** The wide scan XPS spectra of r-MnFePO$_4$@PhG catalyst.

Table S1: The obtained composition of r-$MnFePO_4$@PhG from its wide scan XPS spectrum.

| Sample | P | C | O | Mn | Fe |
|---|---|---|---|---|---|
| r-$MnFePO_4$@PhG | 1.32 | 69.94 | 26.79 | 0.34 | 1.64 |

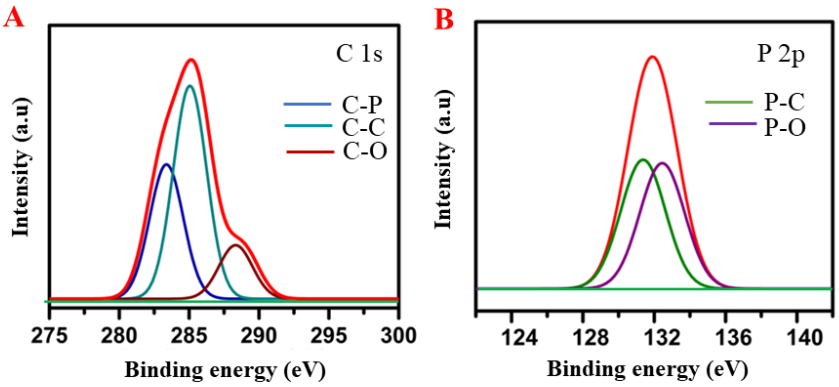


**Figure S4** The deconvoluted high-resolution XPS spectra of (A) C 1s (B) P 2p peaks in the r-$MnFePO_4$@PhG catalyst.

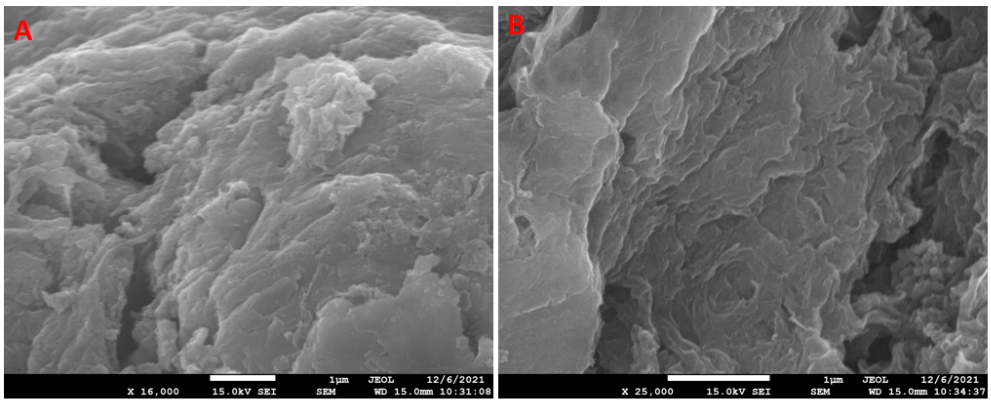


**Figure S5** SEM image of (A) m-$MnFePO_4$@PhG and (B) r-$MnFePO_4$@PhG catalyst.

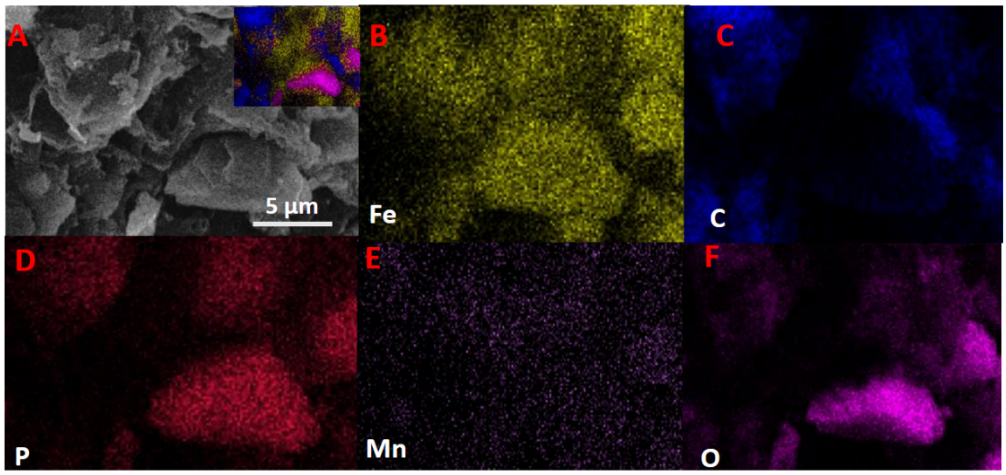


**Figure S6** (A) SEM image and Elemental mapping of (B) Fe, (C) C, (D) P, (E) Mn, and (F) O contents in r-$MnFePO_4$@PhG catalyst.

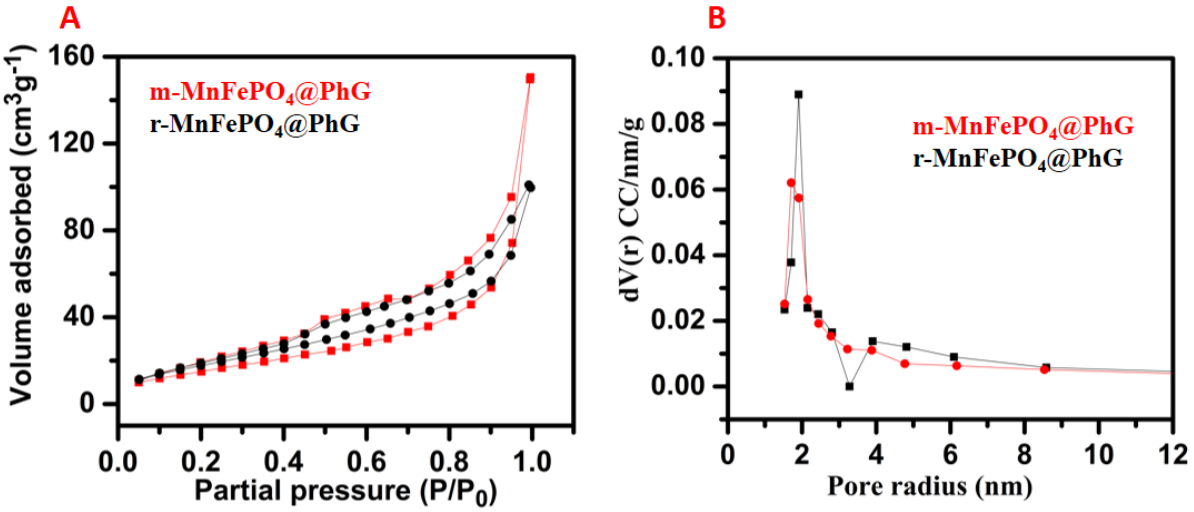


**Figure S7** (A) $N_2$ adsorption-desorption isotherm (B) pore size distribution of the as-prepared m-$MnFePO_4$@PhG and r-$MnFePO_4$@PhG catalysts

**Determination of Electrochemically active surface area (ECSA)**

The electrochemical active surface area (ESCA) was analyzed from double-layer capacitance ($C_{dl}$) method by carrying out cyclic voltammetry (CV) in the confined potential window of the non-faradaic region of 0.96–0.86 V vs. RHE in 0.1M KOH at various scan rates of 2, 5, 10, 20, and 50 mV $s^{-1}$. Then, the double layer capacitance ($C_{dl}$) was assessed from the slope of the linear regression between the current density differences ($\Delta j/2 = (j_a - j_c)/2$) in the middle of the potential window of CV curves versus the scan rates.

The ECSA of the prepared catalysts were calculated from $C_{dl}$ according to the following equation:

$$ECSA = \frac{C_{dl}}{C_s}$$

Here Cs is the specific capacitance of the material. For our estimation, we have used a specific capacitance Cs of 0.04 mF $cm^{-2}$ for 0.1 M KOH. [1,2]

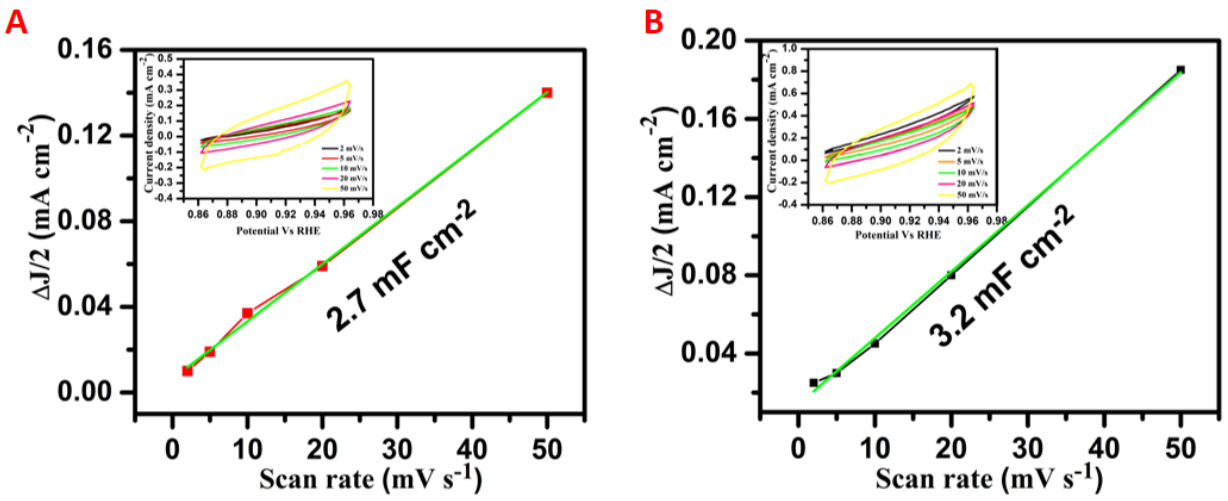


**Figure S8:** Double-layer capacitance ($C_{dl}$) of (A) m-$MnFePO_4$@PhG (B) r-$MnFePO_4$@PhG determined by plotting capacitive currents as a function of scan rates obtained by carrying out CV at scan rates from 2 to 50 $mVs^{-1}$ in a potential window of 0.96–0.86 V vs. RHE, as shown in the inset.

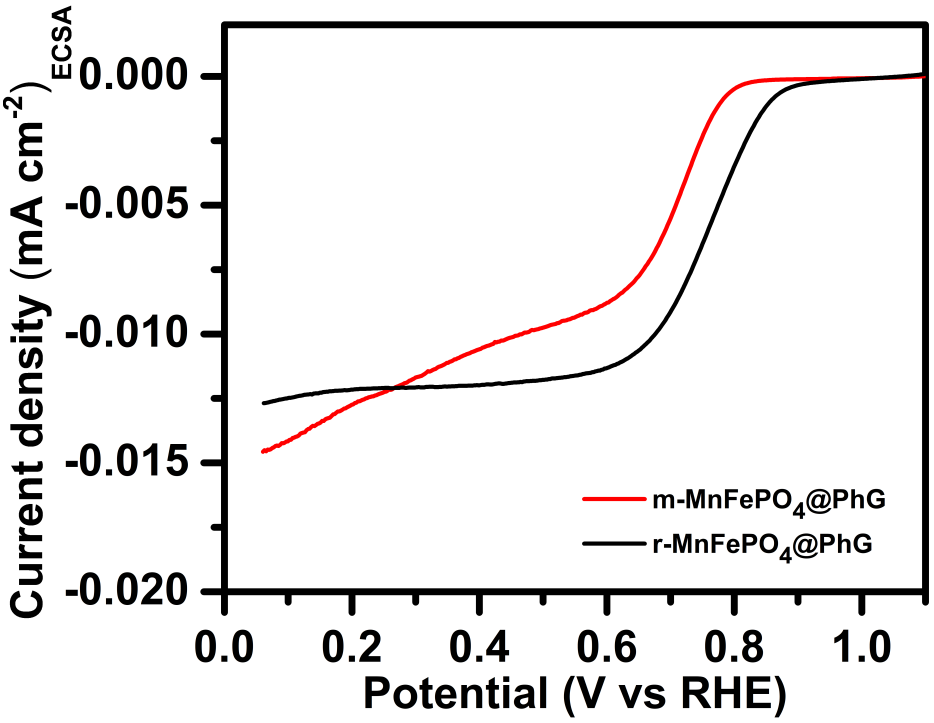


**Figure S9**: ECSA normalized ORR polarization curve of m-$MnFePO_4$@PhG and r-$MnFePO_4$@PhG in 0.1M KOH

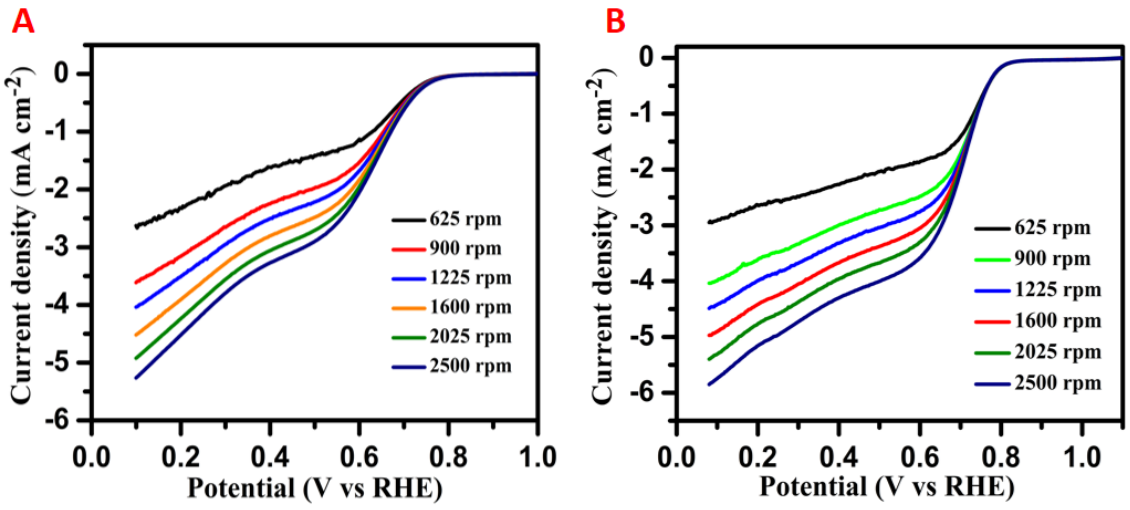


**Figure S10** LSV curves at different rotation speeds (A) b-$FePO_4$@PhG (B) m-$MnFePO_4$@PhG

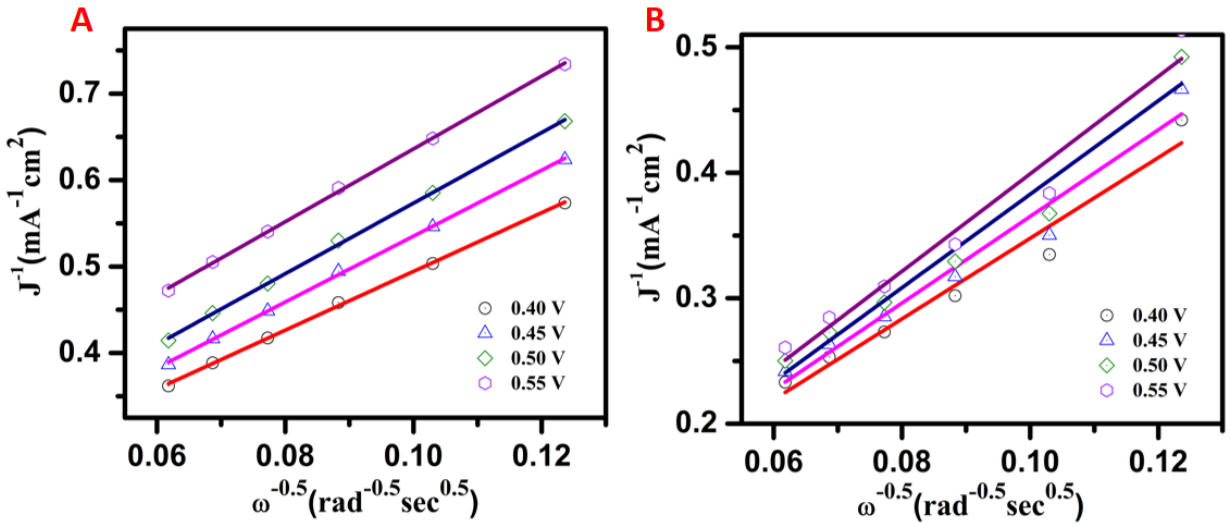


**Figure S11** K-L plots at various potentials of (A) b-$FePO_4$@PhG (B) m-$MnFePO_4$@PhG

**Table. S2** K-L plot parameters of b-$FePO_4$@PhG, m-$MnFePO_4$@PhG, and r-$MnFePO_4$@PhG

**(A) b-$FePO_4$@PhG**

| Potential (V vs RHE) | Slope | Intercept | n | $J_k$ (mA $cm^{-2}$) |
|---|---|---|---|---|
| 0.55 | 4.21081 | 0.214 | 2.01 | 4.67 |
| 0.50 | 4.08484 | 0.164 | 2.08 | 6.09 |
| 0.45 | 3.8161 | 0.153 | 2.23 | 6.53 |
| 0.40 | 3.40055 | 0.154 | 2.5 | 6.49 |

**(B) m-$MnFePO_4$@PhG**

| Potential (V vs RHE) | Slope | Intercept | n | $J_k$ (mA $cm^{-2}$) |
|---|---|---|---|---|

| | | | | |
|---|---|---|---|---|
| 0.55 | 3.88454 | 0.163 | 2.19 | 6.12 |
| 0.50 | 3.72728 | 0.161 | 2.28 | 6.21 |
| 0.45 | 3.45443 | 0.137 | 2.46 | 7.29 |
| 0.40 | 3.21625 | 0.128 | 2.64 | 7.81 |

**(C) r-MnFePO$_4$@PhG**

| Potential (V vs RHE) | Slope | Intercept | n | $J_k$ (mA cm$^{-2}$) |
|---|---|---|---|---|
| 0.55 | 2.55551 | 0.156 | 3.33 | 6.41 |
| 0.50 | 2.5405 | 0.140 | 3.33 | 7.14 |
| 0.45 | 2.51173 | 0.137 | 3.37 | 7.30 |
| 0.40 | 2.49517 | 0.134 | 3.40 | 7.81 |

**Table. S3** ORR performance parameters of PtC, b-FePO$_4$@PhG, m-MnFePO$_4$@PhG, and r-MnFePO$_4$@PhG

| **Catalysts** | **$E_{onset}$ V vs. RHE** | **$E_{1/2}$ V vs. RHE @ -3 mA cm$^{-2}$** | **Tafel slope (mV·dec$^{-1}$)** | **Limiting current density (mA cm$^{-2}$) at 1600 rpm (0.1 V)** |
|---|---|---|---|---|
| Pt/C | 0.99 | 0.77 | 66 | 5.5 |
| r-MnFePO$_4$@PhG | 0.93 | 0.73 | 70 | 5.16 |
| m-MnFePO$_4$@PhG | 0.84 | 0.61 | 72 | 4.9 |
| b-FePO$_4$@PhG | 0.82 | 0.35 | 80 | 4.5 |

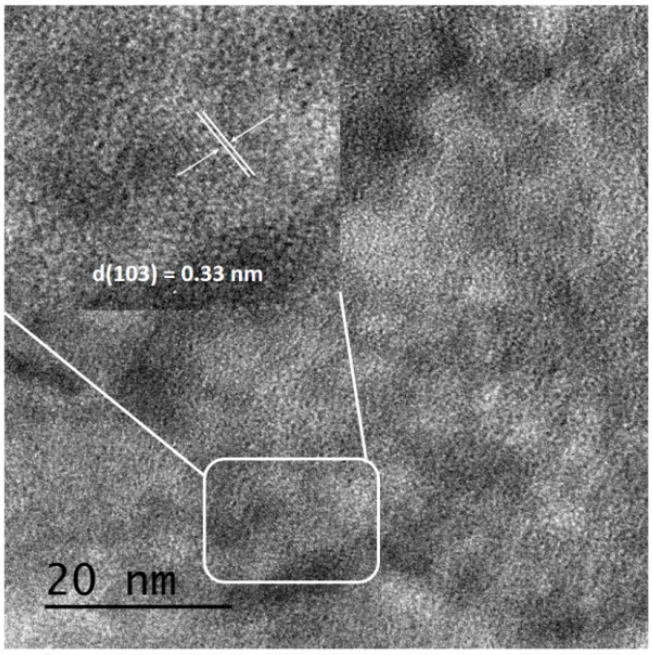


**Figure S12** TEM/HRTEM image of r-$MnFePO_4$@PhG after chronoamperometric measurement showing structural stability of the catalyst

**Table S4:** Comparison of the ORR performance with other non-noble metal based catalysts in literature that are reported in $O_2$-sat. 0.1 M KOH.

| S,No | Catalyst | Onset potential (Eonset) V vs. RHE | Half-wave potential ($E_{1/2}$) V vs. RHE @3 mA $cm^{-2}$ | Tafel slope (mV $dec^{-1}$) | Stability | Reference |
|---|---|---|---|---|---|---|
| 1. | r-$MnFePO_4$@PhG | 0.93 | 0.73 | 70 | Retains 94.7 % of the original current density after ~14h of chronoamperometric (CA) measurement | This work |
| 2. | $Fe_2O_3$/NS-C-800 | 0.97 | 0.81 | 72 | Retains 95.7% current after 10 000 s of CA measurement | 3 |
| 3. | Fe-N/P/C-850 | 1.06 V | 0.86 V | 97.5 | Retains 95.5% of initial current after 30 000 s | 4 |
| 4. | mNC-$Fe_3O_4$@rGO | 0.95 | 0.84 | 67 | Retains 94 % of current after 20 000 s in CA response | 5 |
| 5. | $Fe_3N$/Fe–N–C-900 | 0.847 | 0.773 | 72 | The catalysts reserve 56% of the original current density, after 30 000 s CA testing | 6 |
| 6. | Co/S,N-C | 0.84 | 0.93 | 76 | Stable after 30 000 CV cycles | 7 |

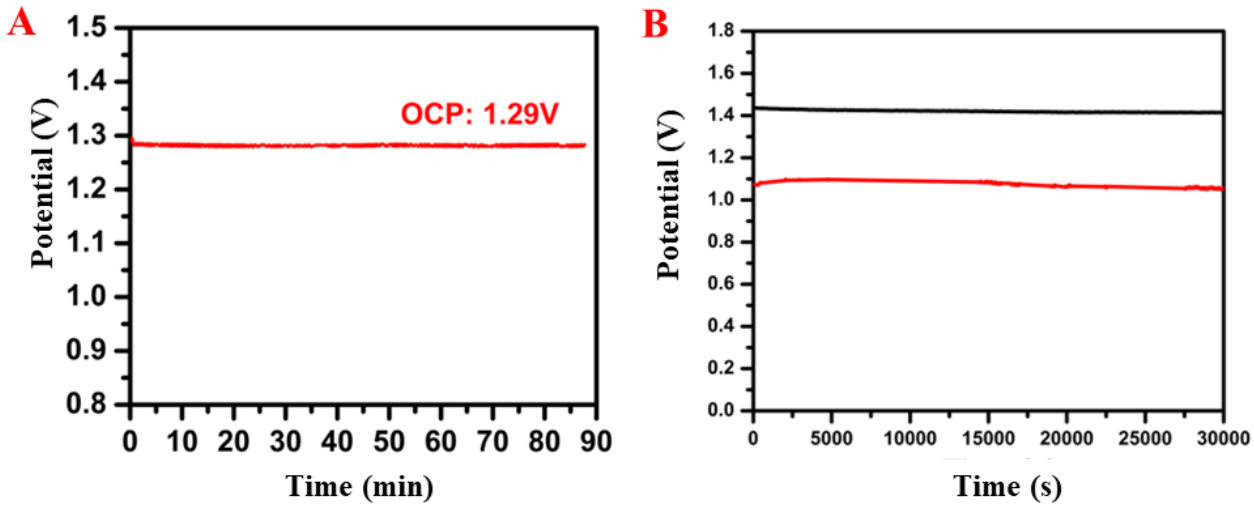


**Figure S13** (A) Open circuit potential measurement of r-$MnFePO_4$@PhG(A) Typical discharge polarization curves of primary Zn-air battery using r-$MnFePO_4$@PhG (red) and Pt/C (black) at a ORR current density of 0.5 $mAcm^{-2}$.

**References:**


1. Yang, X.; Mi, H.; Ren, X.; Zhang, P.; Li, Y., Co/CoP nanoparticles encapsulated within N, P-doped carbon nanotubes on nanoporous metal-organic framework nanosheets for oxygen reduction and oxygen evolution reactions. *Nanoscale Research Letters* **2020,** *15* (1), 1-12.

2. Liu, G.; He, D.; Yao, R.; Zhao, Y.; Li, J., Amorphous NiFeB nanoparticles realizing highly active and stable oxygen evolving reaction for water splitting. *Nano Research* **2018,** *11* (3), 1664-1675.

3. Chao, S.; Xia, Q.; Wang, G.; Zhang, X., Fe2O3 nanoparticles immobilized on N and S codoped C as an efficient multifunctional catalyst for oxygen reduction reaction and overall water electrolysis. *International Journal of Hydrogen Energy* **2019,** *44* (10), 4707-4715.

4. Tang, Y.; Zeng, Z.; Yi, L.; Zhu, S.; Li, X.; Li, H.; Lv, N.; Xu, Y.; Zhang, Q.; Wang, Y., Heteroatom-Anchored Porous Carbon as Efficient Electrocatalyst for Oxygen Reduction Reaction. *Energy & Fuels* **2022**. 36 (4), 2068–2074

5. Zhu, S.; Tian, H.; Wang, N.; Chen, B.; Mai, Y.; Feng, X., Patterning Graphene Surfaces with Iron- Oxide- Embedded Mesoporous Polypyrrole and Derived N- Doped Carbon of Tunable Pore Size. *Small* **2018,** *14* (9), 1702755.

6. Xue, N.; Liu, J.; Wang, P.; Wang, C.; Li, S.; Zhu, H.; Yin, J., Scalable synthesis of Fe3N nanoparticles within N-doped carbon frameworks as efficient electrocatalysts for oxygen reduction reaction. *Journal of Colloid and Interface Science* **2020,** *580*, 460-469.

7. Wang, Z.; Shang, N.; Wang, W.; Gao, S.; Zhang, S.; Gao, W.; Cheng, X.; Wang, C., Atomically dispersed Co anchored on S, N-riched carbon for efficient oxygen reduction and Zn-air battery. *Journal of Alloys and Compounds* **2022,** *899*, 163225.